Korean J. Chem. Eng., **30**(1), 87-94 (2013)
DOI: 10.1007/s11814-012-0120-2

A study on sulfonated poly(arylene ether sulfone) membranes containing two different types of SiO_2 for a high temperature and low-humidified polymer electrolyte fuel cell

Sung-Mi Park*,*, Young-Woo Choi*,†,‡, Tae-Hyun Yang*, Jin-Soo Park**,‡, and Sung-Hyun Kim***,†**

*Fuel Cell Research Center, Korea Institute of Energy Research, Gajeong-dong, Yuseong-gu, Daejeon 305-343, Korea
**Department of Environmental Engineering, Sangmyung University,
300, Anseo-dong, Dongnam-gu, Cheonan-si 330-720, Korea
***Department of Chemical and Biological Engineering, Korea University, Anam-dong, Seongbuk-gu, Seoul 136-701, Korea
(*Received 17 May 2012 • accepted 19 July 2012*)

Abstract−Two different types of silica oxide were prepared as filler in sulfonated polymers for fuel cell applications operated under water deficient environment. SiO_2 nanoparticle and thiol-embedded SiO_2 nanoparticles were mechanically mixed with sulfonated (arylene ether sulfone) solutions, and then the mixtures were cast to prepare composite membranes. The composite membranes with different amount of SiO_2 were prepared to investigate the effect of two types of SiO_2 nanoparticles on ionic conductivity with relative humidity at 120 °C. In addition, ion exchange capacity, water uptake, thermogravitational analysis, differential scanning calorimetry were studied. As results, the composite membranes containing thiol-embedded SiO_2 showed better water-channel forming ability at low relative humidity less than 50% in this study. Under full hydration of the composite membranes, the composite membranes containing pure SiO_2 nano-particles have higher ionic conductivity since the thiol-embedded SiO_2 might cause steric hindrance to make water channel well connected. Thus, below 50% relative humidity, the composite membranes containing 10 wt% of thiol-embedded SiO_2 showed the best ionic conductivity. It is very promising for polymer electrolyte fuel cells operated normally under 50% relative humidity at cathode.

Key words: Silica, Composite Membrane, Proton Conductivity, Low-humidified, Polymer Electrolyte Membrane Fuel Cell

INTRODUCTION

The polymer electrolyte membrane fuel cell (PEMFC) is a very promising technology because it offers a high efficiency with relatively low operation temperature to the other fuel cells such as solid oxide fuel cell and molten carbon fuel cell and even rapid start-up. It is also attracted as an environmental friendly power source overcoming the Carnot limitation of combustion engines. Typically, perfluorinated polymers such as Nafion (DuPont) and Aquivion (Solvay) are used for PEMFC. The perfluorinated membranes have many advantages such as chemical and mechanical stability in severe environments and high proton conductivity when fully hydrated less than 100 °C. However, they are very expensive due to the toxic and complicated production process. Also, they lead to low performance for high temperature fuel cell due to low glass transition temperature. These drawbacks have prompted research into alternative membranes based on aromatic hydrocarbon polymers. Many researchers have developed various aromatic polymer electrolytes such as sulfonated polysulfone (SPS), sulfonated poly(ether ehter ketone) (SPEEK), sulfonated polyphenylquinoxaline (SPPQ), and sulfonated poly(arylene ether sulfon) (SPAES) [1-3,23-25]. However, the water content and the proton conductivity of the hydrocarbon membranes decrease rapidly according to decreasing humidification below 50% at high temperature. Generally, in case of random copolymers, the proton conductivity decreases under high temperature and low-humidified conditions because the water clusters forming consecutive proton-conducting pathways sharply decrease. To increase consecutive proton-conducting pathways, bibulous inorganic materials can be employed into polymer electrolytes (Fig. 1). Many researchers have therefore focused on organic-inorganic composite membranes which have the high water contents and proton conductivity under low humidified conditions. Recently, the composite membranes have been prepared by the addition of inorganic materials such as silica, titania, zirconia, mixed silicon-titanium oxides, zeolites, and montmorillonite in the Nafion membrane [5-10,13-16,21]. They showed high proton conductivities and cell performances when operated under 100 °C and low humidified conditions less than 50%. As using hydrocarbon based polymers such as sulfonated poly(ether ether ketone)-silica membranes, polyvinylidene fluoride-silica membranes and polyethylene glycol-silica have been also developed for various applications. [11,19,20]. However, studies on composite membranes consisting of SPAES with silica have not been investigated so much even though SPAES has higher thermal properties than those of Nafion or other hydrocarbon polymers such as SPEEK and SPS [1,12,15]. Therefore, the composite membranes were prepared with SPAES containing two different types of silica to enhance the property of the membranes under low humidified conditions over 100 °C in this study. One is the composite membranes with SiO_2 nanoparticles dispersed in SPAES. The other is the composite membranes with 3-mercaptopropyl silica (thiol-embedded SiO_2) gel dis-

†To whom correspondence should be addressed.
E-mail: cozmoz67@kier.re.kr, kimsh@korea.ac.kr
‡These authors equally contributed to this paper.

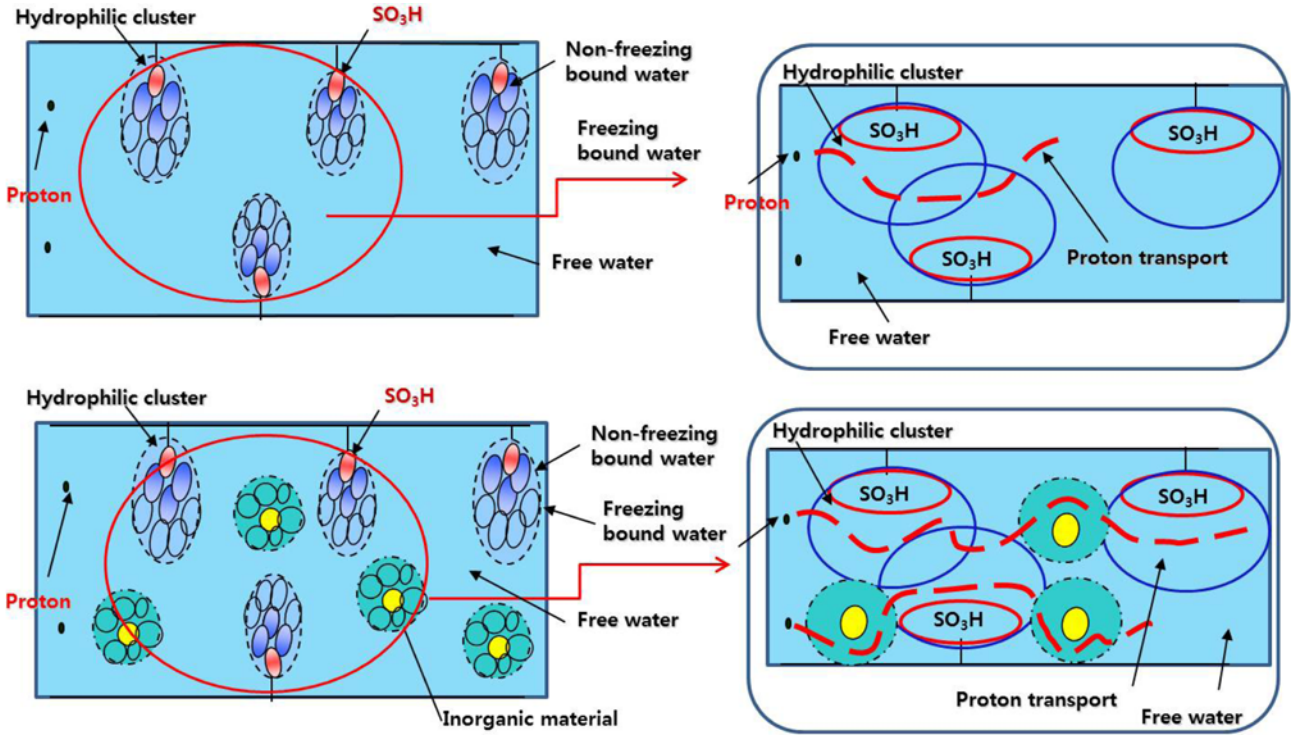

Fig. 1. Proton conducting mechanism in the prepared composite membranes.

persed in SPAES. SiO_2 is normally used as a filler to improve water trapping, being able to get good ionic conductivity under low external relative humidity. Mainly, the ability to enhance ionic conductivity under low external relative humidity between SiO_2 and thiol-embedded SiO_2 was compared in terms of ion exchange capacity, ionic conductivity, water content, DSC, TGA and SAXS.

EXPERIMENTAL SECTION

1. Materials

1-1. Synthesis of Sulfonated Poly(Arylene Ether Sulfone) (SPAES)

SPAES copolymers were synthesized via direct copolymerization using 4,4′-biphenol (BP), Dichlorodiphenyl sulfone (DCDPS), and Sulfonated dichlorodiphenyl sulfone (SDCDPS). The DCDPS, SDCDPS, BP, and K_2CO_3 were reacted in a three-necked flask with 40 mL of *N*-methyl- 2-pyrrolidone (NMP) and 30 mL of toluene. The solution was refluxed at 135 °C for 6 h to dehydrate the mixture. N_2 was purged slowly during the reaction. After completion of dehydration, toluene in the flask and dean-stark trap was removed. The reaction temperature was then slowly increased to 195 °C and maintained for 24 h to complete copolymerization. The prepared SPAES copolymer was cooled to room temperature and precipitated in deionized water. After being washed several times with deionized water, the precipitated copolymer was dried in a vacuum oven

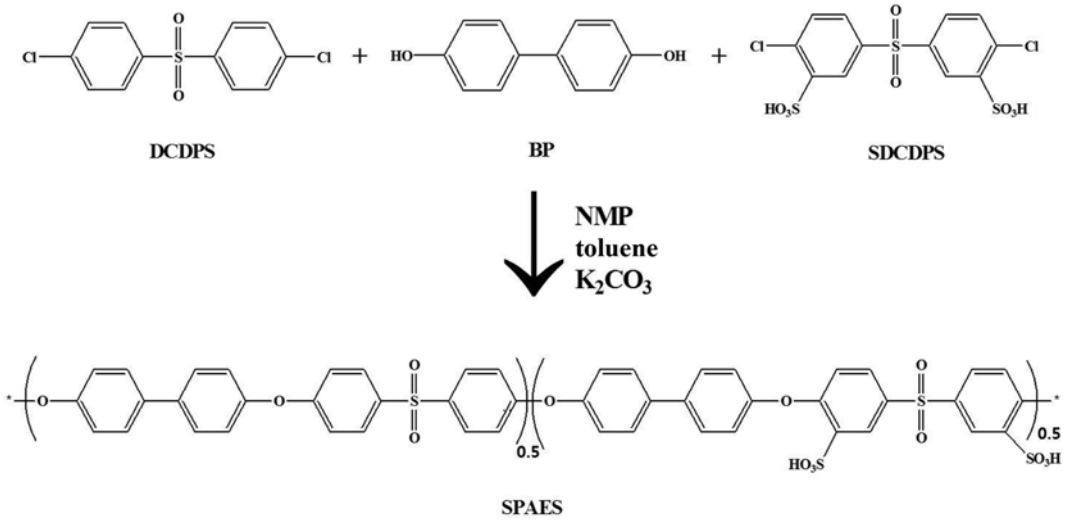

Fig. 2. Schematics of the SPAES preparation.

Table 1. Properties of pure and thiol-embedded SiO_2 particles

	Pure silica	Thiol-embedded silica
Form	Powder	Powder
Particle size	0.2-0.3 μm (aggregate)	Submicron (after grinded)
Surface area	200 m^2/g	500 m^2/g
Thiol function group	-	0.5 to 0.8 mmol/g

at 120 °C for 24 h (Fig. 2).

1-2. Preparation of Nano-SiO_2 Particles

Pure silica and thiol-embedded silica were purchased from Sigma and TCI, respectively. They were used with no further purification. The physical properties of the silica particles are summarized in Table 1. Prior to the use of the particles for preparation of composite membranes, they were ground by mortar and pestle to crush aggregates of the silica particles.

2. Preparation of Composite Membranes

2-1. Preparation of Highly Dispersed SiO_2/SPAES Composite Membranes

The SPAES copolymer was dissolved in NMP to form 10 wt% solutions. The SiO_2 nanoparticles were added with respect to the various concentrations (0-20 wt%) of the SPAES solution. The highly dispersed mixed solution was poured on a petri-dish and dried in a vacuum oven at 120 °C for 24 h. The dried composite membranes were peeled off from the substrate with deionized water. The composite membranes were protonated in 2 N HCl for 12 h [4]. The schematic process is described in Fig. 3.

2-2. Preparation of Thiol-embedded SiO_2/SPAES Composite Membranes

The SPAES copolymers were dissolved in NMP to form 10 wt% solutions. The 3-mercaptopropyl Silica gel was added with respect to the various concentration (0-20 wt%) to the SPAES solution. The highly dispersed mixed solution was poured on a petri-dish and dried in a vacuum oven at 120 °C for 24 h. The dried composite membranes were peeled off from the substrate with deionized water. The composite membranes were protonated in 2 N HCl for 12 h [4]. The schematic process is described in Fig. 3.

3. Characterization of the Prepared Membranes

3-1. Proton Conductivity

The proton conductivity for the fully hydrated membranes at room temperature of the prepared composite membranes was measured by EIS with a Solartron 1260 frequency response analyzer (FRA) using an in-plane four-electrode configuration. Also, the proton conductivity at 120 °C with the various humidifications (20-90%) was measured by a high temperature conductivity test system, BT552, of Bekktech (USA). The Proton conductivity was calculated using the following Eq. (1):

$$\text{Proton conductivity} = \frac{L}{R \times A}(S \cdot cm^{-1}) \quad (1)$$

Where, R is the measured membrane resistance, L is the distance between working and counter platinum wire electrodes, and A is the cross-section area of the membrane.

3-2. Ion Exchange Capacity

The quantity of acid equivalents per gram of polymer can be obtained by the following steps. First, the membrane in the acid form was immersed in 3.3 N NaCl solution to convert sulfonic acid to sodium form. Next, the released H^+ was back titrated with a 0.01 N NaOH solution using phenolphthalein as indicator; meanwhile, the volume of NaOH and pH was recorded to determine the equivalence point. The IEC is the equivalents per gram of dry polymer. The ion exchange capacity (IEC) was calculated using the following Eq. (2):

$$IEC = \frac{V \times M}{m_{dry}} \quad (2)$$

Where, IEC is the ion exchange capacity (mequiv./g); V is the added titrant volume at the equivalent point (mL); M is the molar concentration of the titrant; m_{dry} is the dry sample weight (g).

3-3. Water Uptake

The water uptake of each membrane was calculated by the difference between the wet and dry weight of the membrane. After

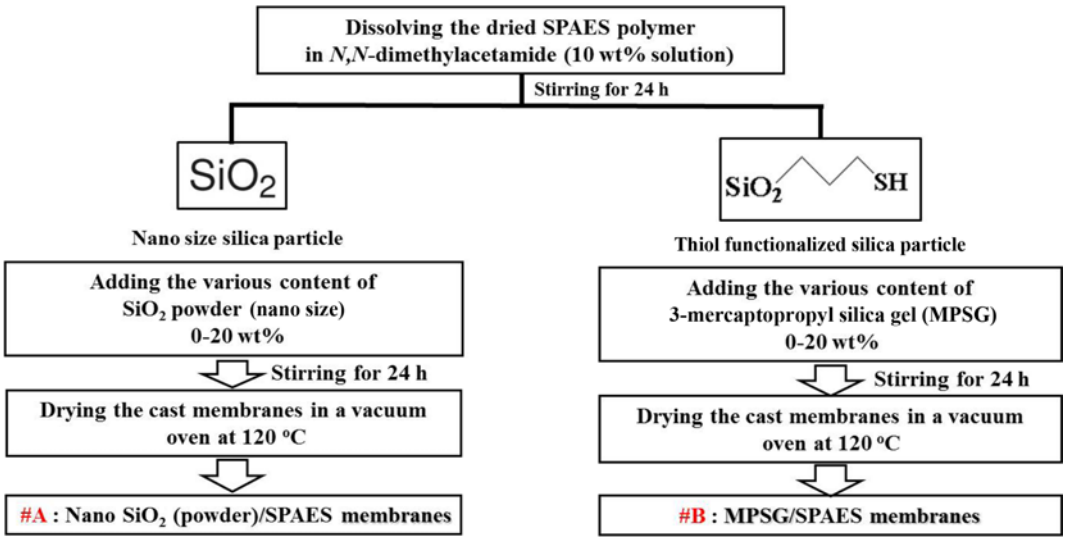

Fig. 3. Preparation method for the composite membranes.

the membrane swelled in distilled water for 24 h at room temperature, the surface of the wet membrane was wiped and weighed quickly. Then the membrane was kept in an oven at 120 °C for 2 h and the dry membrane was weighed. The water uptake was calculated using the following Eq. (3):

$$\text{Water uptake} = \frac{(W_{wet} - W_{dry})}{W_{dry}} \times 100(\%) \quad (3)$$

Where, W_{wet} is the weights of wet membrane; W_{dry} is the weights of dry membrane.

3-4. Thermo Gravimetric Analyzer (TGA)

TGA studies on membranes were carried out to estimate thermal characteristics and to confirm the content of the impregnated inorganic matters in the prepared composite membranes using TGA N-1000. Specimens having typical weights of 4-5 mg were used for TGA measurements. Thermograms were obtained at a constant heating rate of 10 °C /min from room temperature to 800 °C under nitrogen atmosphere. The weight loss shown in the 100 °C represents evaporation of free water in each membrane. The content of the inorganic matters for each sample was calculated from the remaining weight over 700 °C.

3-5. Differential Scanning Calorimetry (DSC)

DSC studies on membranes were carried out to evaluate the state of water in each membrane using DSC 131 EVO. Prior to analysis, the composite membranes were swollen in distilled water for 24 h and then were dried at room temperature. Heat flows were obtained at a constant heating rate of 10 °C/min in the temperature range of room temperature to 250 °C under nitrogen atmosphere. The heat absorption peaks based on bound water were observed from 100-120 °C. The enthalpy by bound water in each membrane was calculated from the area at the heat absorption peak.

3-6. Small-angle X-ray Scattering (SAXS)

Morphology characterization of the membranes was studied by the small-angle X-ray scattering (SAXS). SAXS experiments were performed on a Rigaku D/max-2500 (5 kW) with an image plate system equipped using X-rays with a wavelength of 1.5406 Å. All measurements were at ambient vapor pressure.

RESULTS AND DISCUSSION

Fig. 4 shows the variations of ionic conductivity and water uptake as a function of the amount of SiO_2 in the composite membranes including SiO_2 nanoparticles and thiol-embedded SiO_2 nanoparticles under full hydration. Both the composite membranes with SiO_2 nanoparticles (A membrane) and thiol-embedded SiO_2 nanoparticles (B membrane) show a decrease in ionic conductivity and water content as the amount of SiO_2 increases. This decrease in ionic conductivity and water content is mainly due to the decrease in the fraction of the sulfonated polymer (i.e., SPAES) per unit membrane weight by the addition of SiO_2 nanoparticles. The main water holding ability inside the composite membrane is due to sulfonic acid group of the sulfonated polymer. Thus, the decrease in water content of the composite membranes is observed even though the SiO_2 as water trapper is added to the sulfonated polymer. The ionic conductivity of the A membranes for all the amount of SiO_2 shows higher values than those of the B membranes. It is inferred that the mechanical mixing of pristine SiO_2 nanoparticles to the sulfonated polymer

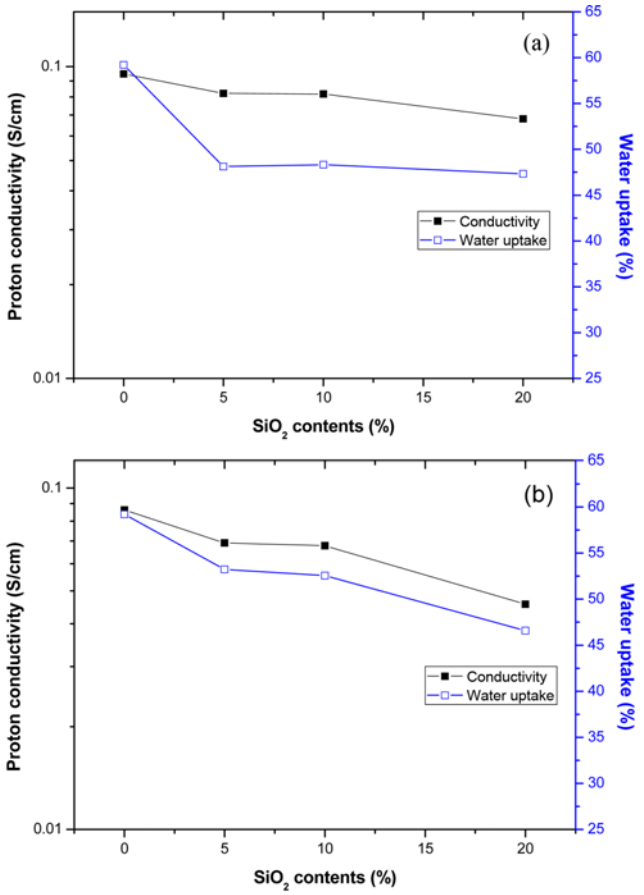

Fig. 4. Water uptake and proton conductivity under fully hydrated condition at room temperature for the prepared composite membranes.

Table 2. Water uptake and IEC of the prepared composite membranes

Calculated content of inorganic matter (wt%)	IEC (meq./g)		Water uptake (%)	
	#A	#B	#A	#B
0	1.510	1.510	59.2	59.2
5	1.572	1.373	48.12	43.48
10	1.471	1.384	48.33	52.55
20	1.386	0.972	47.33	46.58

is better to enhance ionic conductivity than that of thiol-embedded SiO_2 nanoparticles. It means that pristine SiO_2 nanoparticles make well connected ionic pathway in the composite membrane, but thiol-embedded SiO_2 nanoparticle less connected one probably due to the steric hindrance of thiol ended propylene linkage to SiO_2. This is well matched with the results of water uptakes for each membrane under full hydration at room temperature described in Table 2. As increasing the amount of SiO_2, ion exchange capacity and water uptake tend to decrease.

Fig. 5 shows the ionic conductivity with external relative humidity. The composite membranes make water clusters built by the water holding parts such as sulfonic acid groups of the sulfonated polymers as well as two types of SiO_2 nanoparticles for ionic conduction. The main ionic conduction is made by water containing region.

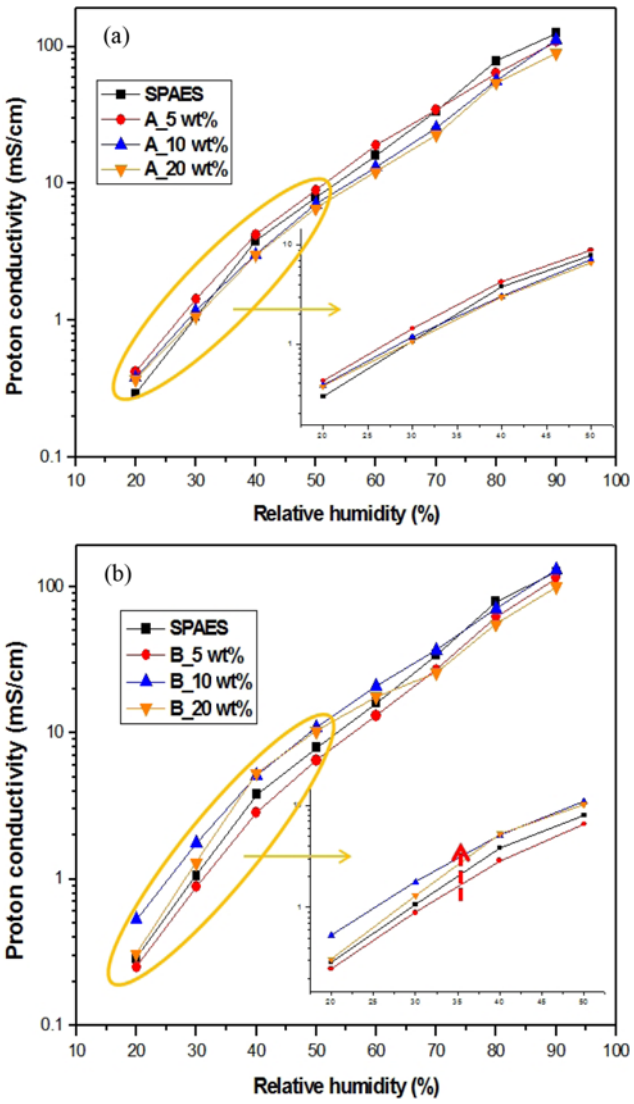

Fig. 5. The proton conductivities at 120 °C with the various relative humidity of the prepared composite membranes: (a) A membranes, (b) B membranes.

Thus, as decreasing external relative humidity, the decrease in ionic conductivity is a quite normal phenomenon for sulfonated polymers including inorganic particles. The A membranes with 5 wt% of SiO_2 show the best ionic conductivity below 70% relative humidity in Fig. 5(a). The A membranes with 10 and 20 wt% of SiO_2 for all relative humidity have lower ionic conductivity even than that of the pristine SPAES. It is assumed that it is difficult to make well connected network above 5 wt%, in simple mean, there might be partial aggregation, not dispersed homogeneously. However, there is no significant difference of ionic conductivity between the pristine SPAES and the A membranes. Interestingly, as shown in Fig. 5(b), it is noted that the B membranes with 10 wt% of thiol-embedded SiO_2 show significantly higher ionic conductivity than those without thiol-embedded SiO_2 and with 5 wt% one. In case of the B membrane with 20 wt% of thiol-embedded SiO_2, the ionic conductivity in the range of 40-50% relative humidity for the B membrane with 20 wt% is similar to that with 10 wt%. Additionally, for the B membranes containing 0, 5 and 20% of thiol-embedded SiO_2, low ionic conductivities were measured, but the B membrane containing 10 wt% showed the exceedingly high ionic conductivity even that that of the A membranes with 5 wt% of SiO_2 nanoparticles which has the highest ionic conductivity at 20% relative humidity.

The absolute ionic conductivity of the A membranes shows higher than that of the B membranes for all the amount of SiO_2 under full hydration, but below 50% relative humidity the absolute ionic conductivity of the B membranes exceeds that of the A membranes. Moreover, a difference in ionic conductivity between pristine SPAES and the A membranes has lower than that between pristine SPAES and the B membranes. It is believed that thiol-embedded SiO_2 makes a better ability to keep water channel well-connected under water deficiency environment. It is inferred that composite membranes containing thiol-embedded SiO_2 is very promising for nonsensitive fuel cell membranes to external relative humidity if they have the absolute ionic conductivity. Thus, further works to make an effort to increase ionic conductivity for composite membranes with thiol-embedded SiO_2 nanoparticles are necessary.

Shao et al. have reported that the SiO_2-Nafion composite membranes showed lower proton conductivity than pristine Nafion membrane under 100% RH as the content of SiO_2 particle increased [5]. However, at low relative humidity, the composite membrane distinguishably had higher proton conductivity than pristine Nafion

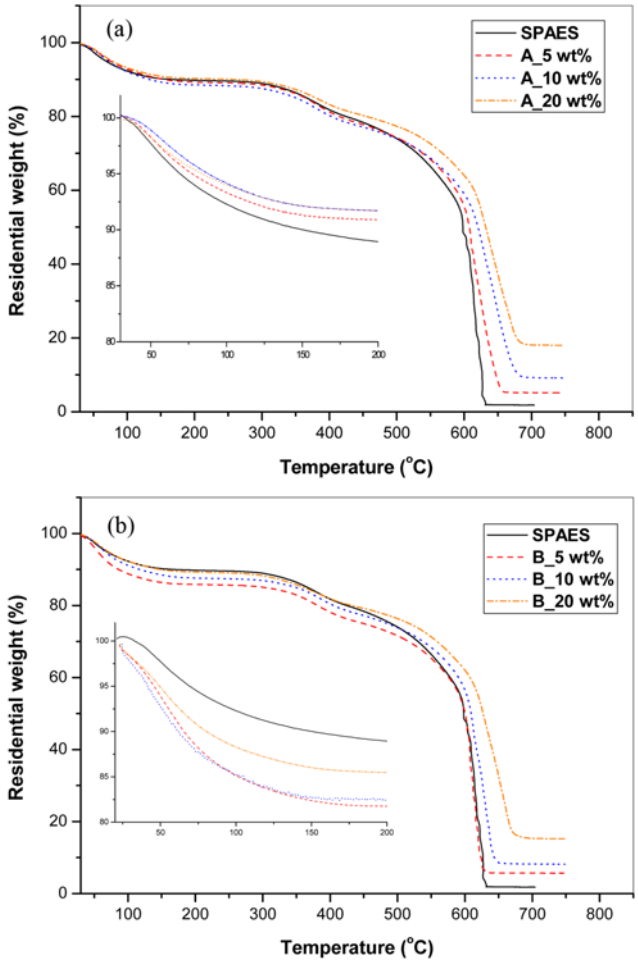

Fig. 6. TG analysis of the prepared composite membranes: (a) A membranes, (b) B membranes.

membrane. This behavior is because a perfluorosulfonic acid polymer like Nafion easily loses water, and finally its proton conductivity significantly decreases. Thus the introduction of SiO_2 particles in the polymer is very good at enhancing proton conductivity at lower relative humidity. In this manuscript, however, the authors used the aromatic hydrocarbon polymer which is insensitive to losing water under lower relative humidity. A decrease in proton conductivity for aromatic hydrocarbon membranes is relatively insensitive compared to Nafion membranes. The composite membrane containing 10 wt% of thiol-embedded SiO_2 in this study showed significantly higher proton conductivity below 50% relative humidity. The main reason why the ionic conductivity of the composite membranes containing pure or thiol-embedded SiO_2 has not changed significantly was that the authors used the aromatic hydrocarbon polymer.

Fig. 6 shows the thermogravitational analyses of the composite membranes (i.e., A and B membranes). All the curves show typical trends represented in composite membranes including inorganics: i) the first decrease in weight due to absorbed water up to 150 °C, ii) the second decrease due to the decomposition of sulfonic groups of the sulfonated polymer from 150 to 450 °C, iii) the third decrease due to the decomposition of the main chain of the polymer from 450 to 600 °C, and iv) the final constant behavior in weight with temperature over 600 °C. There is no significant difference between the A and the B membranes. Using the final constant behavior in weight, real weights introduced to the composite membranes can be calculated. As summarized in Table 3, it can be confirmed that a very similar amount of SiO_2 expected is introduced properly to the composite membranes.

To investigate the effects of the SiO_2 nanoparticles on ionic aggregation, we measured the enthalpy change using differential scanning calorimetry (DSC). The enthalpy change, ΔH, is an indicator of the sum of the degree of ionic aggregations and the degree of crystalline of composite membranes, i.e., an indicator of the degree of phase separation. Therefore, a higher ΔH is required to overcome higher ionic interactions and results in higher mobility of the chains due to stronger ionic interaction. Table 4 summarizes the results of the temperatures at maximum peak heat flow and ΔH values when the heat flow changed around the temperature for each composite membrane. In general, the temperature at maximum peak heat flow is known as transition temperature, resulting in bound water clustered strongly with sulfonic acid groups in polymer electrolytes [27]. In addition, at the transition temperature, the largest endothermic reaction is necessary to break the binding energy between the bound water and sulfonic acid groups. Table 4 shows that transition temperatures, and ΔH values well corresponded to the related peaks. In case of the B membrane containing 10 wt% of thiol-embedded SiO_2, with a peak temperature around 113 °C, the largest endotherm corresponds to the dissociation of ionic aggregations. These results clearly establish that the B membrane containing 10 wt% of thiol-embedded SiO_2 maintains a stronger ionic interaction compared to the other membranes including the pristine SPES membrane. These are also very well accordant with the results of the conductivity as shown in Fig. 5. According to Gierke et al., an increase in the water absorbed by a Nafion polymer membrane leads to an increase of the number of sulfonic groups per aggregate and an increase in the size of the aggregate, which results in more highly organized ionic clusters and more cohesive ionic interaction [28]. However, the results of IEC in this study showed that the sulfonic group per unit weight of SPAES random copolymers decreases with increasing SiO_2 content due to the characteristics of nanophase-separated morphology of the hydrophobic and hydrophilic domains of hydrocarbon-type membranes. Therefore, we can assume that a stronger ionic interaction is attributed to the higher connectivity of ionic groups. The temperature at the endothermic peak of the B membrane containing 10 wt% of thiol-embedded SiO_2 is the lowest than those of the other membranes. Almeida and Kawano [29] demonstrated that an increase of the degree of hydration in a polymer membrane increases the enthalpy changes and ΔH, and decreases the temperature at the endothermic peak. A decrease in the temperature at the peak can be associated with a water plasticizing effect in the composite membrane. The adsorbed bound water increases the free volume, and also increases the chain mobility. This results in a decrease in the peak temperature. Our experimental results are in good agreement with the results reported by Almeida and Kawano [29].

Table 3. TG analysis of the prepared composite membranes

Calculated content of inorganic matter (wt%)	Measured content of inorganic matter (wt%)	
	#A	#B
0	1.64	1.64
5	5.25	6.17
10	9.53	8.62
20	18.09	15.84

Table 4. DSC analysis of the prepared composite membranes

Calculated content of inorganic matter (wt%)	H (J/g)		Max. peak (°C)	
	#A	#B	#A	#B
0	200.7	200.7	120.7	120.7
5	276.4	289.6	119.2	126.9
10	207.3	373.3	128.3	113.9
20	254.7	282.8	113.9	127.1

The morphology of water swollen sulfonated membranes at the ambient vapor pressure has been frequently studied by small-angle X-ray scattering (SAXS), and the overall SAXS profile has been reported to show the following general features [30-34]:

- An upturn of the intensity I(q) at very small q ($<10^{-2}$ Å^{-1}) values, which is strongly related to the ionic clusters. It is generally associated with the long range inhomogeneities in the spatial distribution of the ionic clusters.

- The presence of a small peak (shoulder) centered at intermediate q values is called the matrix peak. The intensity of this peak depends upon the crystalline content of the sulfonated polymer films or the presence of crystallites in the hydrophobic phase.

- The small-angle scattering maximum ("ionomer peak"), which originates from either the shape of the ionic clusters or their spatial distribution. The position of the ionomer peak corresponds to the mean center to center spacing between the ionic clusters.

- The tail region of the SAXS profile shows an asymptotic behavior in the large q-region and follows Porod's law ($I(q) \propto q^{-4}$), which is an indication that the polymer-solvent interface is sharp and it

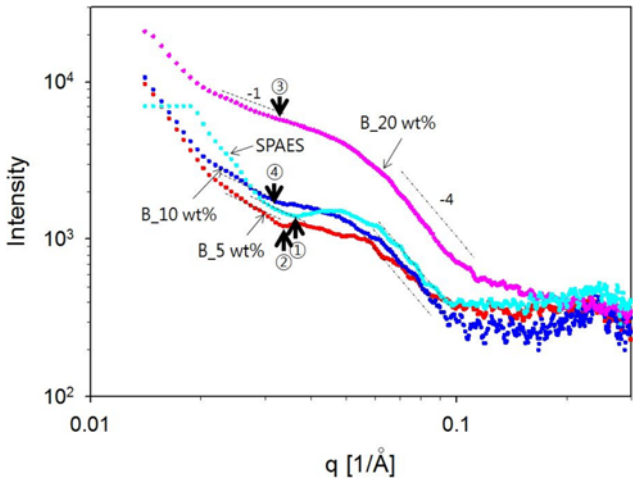

Fig. 7. SAXS curves of the B membranes with various content of SiO_2 at the ambient vapor pressure.

also supports that the phase separation has taken place.

Fig. 7 shows the morphology of the membranes based on SPAES and containing SiO_2 studied by SAXS, and the SAXS spectra show the variation of scattered intensity as a function of the scattering vector q. The SAXS results for the SPAES and SPAES/SiO_2 composite membranes are different and depend upon the content of SiO_2. From the results given in Fig. 7, the following observations can be made:

- A small shoulder related to the matrix peak appears before the -1 slope (shown in Fig. 7 by a dotted line for comparison) of the intensity line in the q region (0.01-0.03) for all the membranes, which is associated with the long range inhomogeneities in the spatial distribution of the ionic clusters.

- The -1 slopes of the intensity line in the q region (0.02-0.04) for all the membranes are shown, which is associated with the crystalline content of the sulfonated polymer films or the presence of crystallites in the hydrophobic phase.

- The broad ionomer peak has been observed for all the membranes. The SPAES shows relatively sharp ionomer peak at q=0.05 $Å^{-1}$ compared to the composite membranes containing SiO_2, but the SPAES/SiO_2 membranes show very broad ionomer peaks. The broadness becomes apparent as the content of SiO_2 increases. The starting points of the ionomer peaks for the membranes after the -1 slope of the intensity line show different, and its order from a higher q value is SPAES, 20 wt%, 5 wt% and 10 wt% SiO_2 composite membranes (see the inset circled numbers shown in Fig. 7). The higher the q values of the starting points are, the higher the maximum q values (q_{max}) of the ionomer peaks are. The observation of the ionomer peak at higher q_{max} values indicates that the size of ionic clusters is smaller. Thus, the order of the membranes consisting of smaller ionic clusters is SPAES, 20 wt%, 5 wt% and 10 wt% SiO_2 composite membranes. The bigger ionic cluster results in better ionic connectivity, thus higher ionic conductivity. These results are fairly in agreement with the conductivity result below 50% RH (note the SAXS spectra measured at ambient vapor pressure, normally 20-50% RH).

- After the position of the ionomer peak, a sharp fall in intensity has been observed for all the membranes in the high q region (0.06-0.1). The slope of the scattered intensity curve in this region is approximately -4 for all the membranes except the membranes containing 5 wt% SiO_2 showing a very narrow range of q-values.

CONCLUSIONS

For automobile applications, proton exchange membrane fuel cells normally use air supply with 50% relative humidity at cathode for operations. From the viewpoint of the fuel cell system, balance of plants (BOPs) should be minimized for total weight and volume because their humidification units make systems complicated and heavier. To overcome this problem, the development of proton exchange membranes with a good ionic conductivity at low relative humidity is essential. In this study, the composite membranes including pure SiO_2 and thiol-embedded SiO_2 were prepared for keeping ionic conductivity good enough to operate under water deficient environment. It was found that the ionic conductivities of the composite membranes containing thiol-embedded SiO_2 under water deficient environment (particularly below 50% relative humidity) were higher than those of the membranes containing pure SiO_2.

ACKNOWLEDGEMENTS

This work was supported by the project, 2009301003003A and 20113020030040, of the Korea Institute of Energy Technology Evaluation and Planning (KETEP) grant and the project, 10037748, of Korea Evaluation Institute of Industrial Technology (KEIT) grant funded by the Korea government Ministry of Knowledge Economy.

REFERENCES

1. K. K. Lee, T. H. Kim, T. S. Hwang and Y. T. Hong, *Membr. J.*, **20**, 278 (2010).
2. Y. T. Goh, R. Patel, S. J. Im, J. H. Kim and B. R. Min, *Korean J. Chem. Eng.*, **26**(2), 518 (2009).
3. S. J. Im, R. Patel, S. J. Shin, J. H. Kim and B. R. Min, *Korean J. Chem. Eng.*, **25**(4), 732 (2008).
4. H. Hagihara, H. Uchida and M. Watanabe, *Eletrochim. Acta*, **51**, 3979 (2006).
5. Z. G. Shao, H. Xu, M. Li and I. M. Hsing, *Solid State Ionics*, **177**, 779 (2006).
6. M. P. Rodgers, Z. Shi and S. Holdcroft, *J. Membr. Sci.*, **325**, 346 (2008).
7. R. Jiang, H. R. Kunz and J. M. Fenton, *J. Membr. Sci.*, **272**, 116 (2006).
8. M. A. Zulfikar and A. W. Mohammad, *J. Matematika Dan Sains*, **11**, 134 (2006).
9. Y. M. Kim, S. H. Choi, H. C. Lee, M. Z. Hong, K. Kim and H. I. Lee, *Eletrochim. Acta*, **49**, 4787 (2004).
10. H. Pu, L. Liu, Z. Chang and J. Yuan, *Eletrochim. Acta*, **54**, 7536 (2009).
11. I. Colicchio, D. E. Demco, M. Baias and M. Moeller, *J. Membr. Sci.*, **337**, 125 (2009).
12. C. H. Lee, K. A. Min, H. B. Park, Y. T. Hong, B. O. Jang and Y. M. Lee, *J. Membr. Sci.*, **303**, 258 (2007).
13. K. T. Park, U. H. Jung, D. W. Choi, K. Chun, H. M. Lee and S. H. Kim, *J. Power Sources*, **177**, 247 (2008).

14. Y. Tominaga, I. C. Hong, S. Asai and M. Sumita, *J. Power Sources*, **171**, 530 (2007).
15. K. S. Yoon, J. H. Choi, Y. T. Hong, S. K. Hong and S. Y. Lee, *Electrochem. Commun.*, **11**, 1492 (2009).
16. Y. Feng, C. Y. Yen, C. M. Ma, S. H. Liao, C. H. Huang and Y. H. Hsiao, *J. Power Sources*, **165**, 692 (2007).
17. F. Wang, M. Hickner, Q. Ji, W. Harrison, J. Mecham, T. A. Zawodzinski and J. E. McGrath, *Macromol. Symp*., **175**, 387 (2001).
18. V. D. Noto, R. Gliubizzi, E. Negro and G. Pace, *J. Phys. Chem. B*, **110**, 24972 (2006).
19. L. Y. Yu, Z. L. Xu, H. M. Shen and H. Yang, *J. Membr. Sci.*, **337**, 257 (2009).
20. H. Y. Chang and C. W. Lin, *J. Membr. Sci.*, **218**, 295 (2003).
21. Y. F. Zhai, H. Zhang, J. Hu and B. Yi, *J. Membr. Sci.*, **280**, 148 (2006).
22. S. Li and M. Liu, *Eletrochim. Acta*, **48**, 4271 (2003).
23. P. Xing, G. P. Robertson, H. D. Guiver, S. D. Mikhailenko, K. Wang and S. Kaliaguine, *Macromolecules*, **37**, 7960 (2004).
24. T. Mikami, K. Miyatake and M. Watanabe, *American Chemical Society*, **2**, 1714 (2010).
25. J. H. Chang, J. H. Park, G. G. Park, C. S. Kim and O. O. Park, *J. Power Sources*, **124**, 18 (2003).
26. R. Lin, B. Li, Y. P. Hou and J. M. Ha, *Int. J. Hydrog. Energy*, **34**, 2369 (2009).
27. T. H. Kim, Y. W. Choi, C. S. Kim, T. H. Yang and M. N. Kim, *J. Mater. Chem.*, **21**, 7612 (2011).
28. T. D. Gierke, G. E. Munn and F. C. Wilson, *J. Polym. Sci., Polym. Phys. Ed*., **19**(11), 1687 (1981).
29. S. H. de Almeida and Y. Kawano, *J. Therm. Anal. Calorim*., **58**, 569 (1999).
30. S. S. Sekhon, J.-S. Park and Y.-W. Choi, *Phy. Chem. Chem. Phy.*, **12**(41), 13763 (2010).
31. S. S. Sekhon, J.-S. Park, J.-S. Baek, S.-D. Yim, T.-H. Yang and C.-S. Kim, *Chem. Mater*., **22**(3), 803 (2010).
32. J.-S. Baek, J.-S. Park, S. S. Sekhon, T.-H. Yang, Y.-G. Shul and J.-H. Choi, *Fuel Cells*, **5**, 762 (2010).
33. S. S. Sekhon, J.-S. Park, E. K. Cho, Y.-G. Yoon, C.-S. Kim and W.-Y. Lee, *Macromol*., **42**(6), 2054 (2009).
34. E.-K. Cho, J.-S. Park, S. S. Sekhon, G-G. Park, T.-H. Yang, W.-Y. Lee, C.-S. Kim and S.-B. Park, *J. Electrochem. Soc*., **156**(2), B197 (2009).